



The Motion and Range of Landslides According to Their Height

Heng Li¹, Zhao Duan^{2*}, Yanbin Wu², Chenxi Dong² and Fasuo Zhao¹

¹College of Geological Engineering and Surveying, Chang'an University, Xi'an, China, ²College of Geology and Environment, Xi'an University of Science and Technology, Xi'an, China

The frequency of catastrophic geological disasters has been increasing significantly, causing tremendous losses of life and property. The study of landslide motion remains incomplete. The variables H/L (ratio of landslide height to length) are often used to describe landslide motion; however, they may also be affected by the height of the landslide itself. To better understand landslide dynamics, this paper aimed to 1) identify the process of landslide motion in relation to height; 2) understand the range of influence of sliding bodies according to height; and 3) construct a formula of landslide disaster range based on the travel distance of the slide center and changes in the center and shape of the sliding body. In this paper, medium-fine quartz sand was used in experiments to observe the movement patterns and sliding body barycenter variations occurring during landslides. We describe the changes that occur during landslides and their deposits' morphological characteristics and barycenter variations with height. Based on these observations, a landslide model is derived. This paper proposes a new method of estimating the effects of landslides, which can help to mitigate the effects of disasters.

Keywords: landslide, falling height, runout distance, sliding body, experiment

OPEN ACCESS

Edited by:

Chong Xu,
Ministry of Emergency Management,
China

Reviewed by:

Siyuan Ma,
China Earthquake Administration,
China

Fanyu Zhang,
Lanzhou University, China

*Correspondence:

Zhao Duan
duanzhao@xust.edu.cn

Specialty section:

This article was submitted to
Geohazards and Georisks,
a section of the journal
Frontiers in Earth Science

Received: 05 July 2021

Accepted: 25 August 2021

Published: 08 September 2021

Citation:

Li H, Duan Z, Wu Y, Dong C and Zhao F
(2021) The Motion and Range of
Landslides According to Their Height.
Front. Earth Sci. 9:736280.
doi: 10.3389/feart.2021.736280

INTRODUCTION

Due to human activities and global climate change, the frequency of catastrophic geological hazards has increased significantly, causing tragic losses of life and property (Berger, McArdell, and Schlunegger 2011; Zhou, Cui, and Yang 2013; Opiso et al., 2016; Aaron et al., 2017; Duan, Yan, et al., 2021; Yan, Duan, and Sun 2021). A variety of geological hazards are related to the rapid diffusion of particulate matter across complex terrain and basement strata, such as landslides, rock collapses, pyroclastic collapses, debris flows, ice and snow collapses, and pyroclastic flows (Dufresne 2012). There have been many studies on landslide runout distance in recent years. For example,

Abbreviations: F_1 , Resultant force on the sliding body at the slanted board phase [N]; F_2 , Resultant force on the sliding body at the horizontal board phase [N]; f_1 , Friction between the sliding body and the slanted board [N]; f_2 , Friction between the sliding body and the horizontal board [N]; G , Gravity [N]; H , Difference in elevation from the rear edge of the initial sliding body to the front toe of the final deposit [mm]; H_d , Height of the final deposit [mm]; H_b , Difference in elevation between the barycenter of the initial sliding body and that of the final deposit [mm]; H_i , Height of the initial sliding body [mm]; L , Horizontal distance from the rear edge of the sliding body at the initial position to the front toe of the final deposit [mm]; L_d , Length of the final deposit [mm]; L_g , Horizontal distance between the barycenter of initial sliding body and that of the final deposit [mm]; L_i , Initial horizontal length of the sliding body [mm]; L_r , Horizontal distance between the barycenter of the final deposit and the trailing edge of the final deposit [mm]; N_1 , Normal force exerted by the slanted board on the sliding body [N]; N_2 , Normal force exerted by the horizontal board on the sliding body [N]; O , Barycenter; S_1 , Distance between the barycenter of the initial sliding body and the boundary line of two boards [mm]; S_2 , Distance from the barycenter of the final deposit and the boundary line of two boards [mm]; W_d , Width of the final deposit [mm]; W_i , Width of the initial sliding body [mm]; M , Effective friction coefficient [*].

Okura et al. used real-scale outdoor rockfall experiments and associated numerical simulations to illustrate the mechanism by which the amount of rockfall affects its runout distance (Yoichi Okura et al., 2000). They also developed a computer simulation model for the dry and non-viscous flow of granular materials and used this to perform response analysis to quantitatively determine the physical properties of the particles and the effect of slope inclination on the distance traveled (Y Okura, Kitahara, and Sammori 2000). More recently, Zou et al. determined the effects of volume, topography, materials, and triggering factor on landslide mobility from 55 catastrophic historical landslides (Zou et al., 2017). Xu et al. presented a data-driven framework for estimating the potential landslide runout distance (Xu et al., 2019).

In landslide dynamics research, the landslide *H*-to-*L* ratio can be used to describe the movement capacity of geological hazards. The smaller the *H/L* ratio, the stronger a landslide's movement ability. There are some differences in the names and formulas used to describe this ratio (Scheidegger 1973; Staron 2008; Lucas, Mangeney, and Ampuero 2014; Crosta et al., 2015). It has been referred to as the "Fahrboschung" (Evans and Clague 1994; Geertsema et al., 2006; Hungr 2006), "reach angle" (Scheidegger 1973; Corominas 1996) "effective friction coefficient" (Staron 2008), and "apparent friction coefficient" (Scheidegger 1973; Bouchut et al., 2015; Duan et al., 2020; H. Q.; Yang et al., 2018; Staron 2008; Magnarini et al., 2019; G.; Wang, Sassa, and Fukuoka 2003; Q.; Yang et al., 2011; Legros 2002). By associating *H/L* with the mass of the sliding body, it has been found that a larger sliding mass body results in a lower *H/L* and stronger landslide movement ability. However, the influences of *H* on the *H/L* ratio and on landslide movement ability have not been systematically studied under the condition that the landslide mass remains unchanged.

Experiments can help to understand the movement mechanism involved in particle flows and have been widely used in research on the movement of geological hazards in recent years. They can also evaluate relevant physical parameters to improve slip distance predictions and verify numerical models (Duan et al., 2020; Iverson, George, and Logan 2016; Ng et al., 2017; H. Q. Yang et al., 2018; Y.-F. Wang et al., 2016). Some experimental studies have focused on the geometry of geohazard deposits in complex geological conditions (Kim et al., 2020; Crosta et al., 2017; Ng et al., 2017; Crosta et al., 2015). For example, Crosta et al. (Crosta et al., 2015; 2017) focused on a landslide collapsing onto an erodible layer or shallow water. Ng et al. (Ng et al., 2017) established a discrete element model to explore the interaction between dry granular flow and rigid barrier deflectors. Pudasaini and Jaboyedoff presented a general analytical model for superelevation in landslide (Pudasaini and Jaboyedoff 2020). Many experimental studies considered the relationship between runout distance and the volume of sliding body. There are still few studies on the variation process of length, width and height of the sliding body.

This article aims to experimentally investigate the displacement and deformation of sliding body during the whole motion. To better understand landslide dynamics, this paper focuses on the following research objectives: 1) to reveal the

evolution of length, width and height of sliding bodies at different landslide heights; and 2) to construct a landslide length prediction formula.

METHODS AND MATERIALS

Slip Sand Experiment

In this paper, changes in the sliding body's motion pattern and center of gravity during a landslide were studied *via* a slip sand experiment. As shown in **Figure 1**, the experimental apparatus consisted of a sandbox, slanted plate, horizontal plate, high-speed camera, and three-dimensional scanner. The sandbox, slanted plate, and horizontal plate were made of Plexiglas. The slanted and horizontal plates had the same dimensions of 1.5 m length and 1.2 m width. The slanted plate could be connected to the horizontal plate at any angle using a bracket. There were two grooves on the slanted plate for fixing the sandbox at any position *via* screws. The sandbox's inner dimensions were 300 mm in length, 150 mm in width, and 120 mm in height. The sandbox was filled from the top with sand and sealed with a breathable cover plate. The bottom of the sandbox featured a swing door with a switch set at the front of the sandbox. When the spring door switch was triggered, the door opened within 0.25 s and the sand in the box would slide out freely without boundary constraint. The millimeter-level 3D dynamic scanner recorded images at 120 frames/s, extracted key point coordinates at eight frames/s, and collected digital elevation model data and positional and morphological data during movement of the sliding body.

Landslide distance is a very complex problem due to the influence of many factors. In order to better clarify the influence of landslide height on landslide runout distance, this paper unified the variables like angle of the landslide and mechanical strength of the soil, simplified the sliding surface, the geomorphology, and ignored the influence of factors like rainfall (water content changes), and earthquake (dynamic loading). This highlighted the effect of landslide height changes on the evolution of the sliding body's length, width, height and barycenter. Most of the landslide angles ranged from 20° to 60°. Smaller landslide angles can lead to a lack of differentiation in landslide heights. In this paper, a larger landslide angle is selected in order to better demonstrate the difference in height. Therefore, the angle of the slanted plate used in this experiment was set to 60°. The volume of the sand body was $5.4 \times 10^3 \text{ cm}^3$. The initial heights of the trailing edge of the sandbox (*H*) were 65, 70, 75, 80, 85, 90, 95, 100, 105, and 110 cm. The experiment was carried out according to the following steps: 1) Fill the sandbox with $5.4 \times 10^3 \text{ cm}^3$ of sand; 2) turn on the high-speed camera and 3D dynamic scanner; 3) trigger the sandbox swing door and let the sand slide down freely; and 4) analyze the motion pattern of the sliding body.

Properties of Sand Samples

Medium-to-fine quartz sand was used as the sliding material because its flow characteristics are similar to those of natural flowslides. This type of sand is widely used in indoor landslide simulation experiments (Viroulet et al., 2013; Crosta et al.,

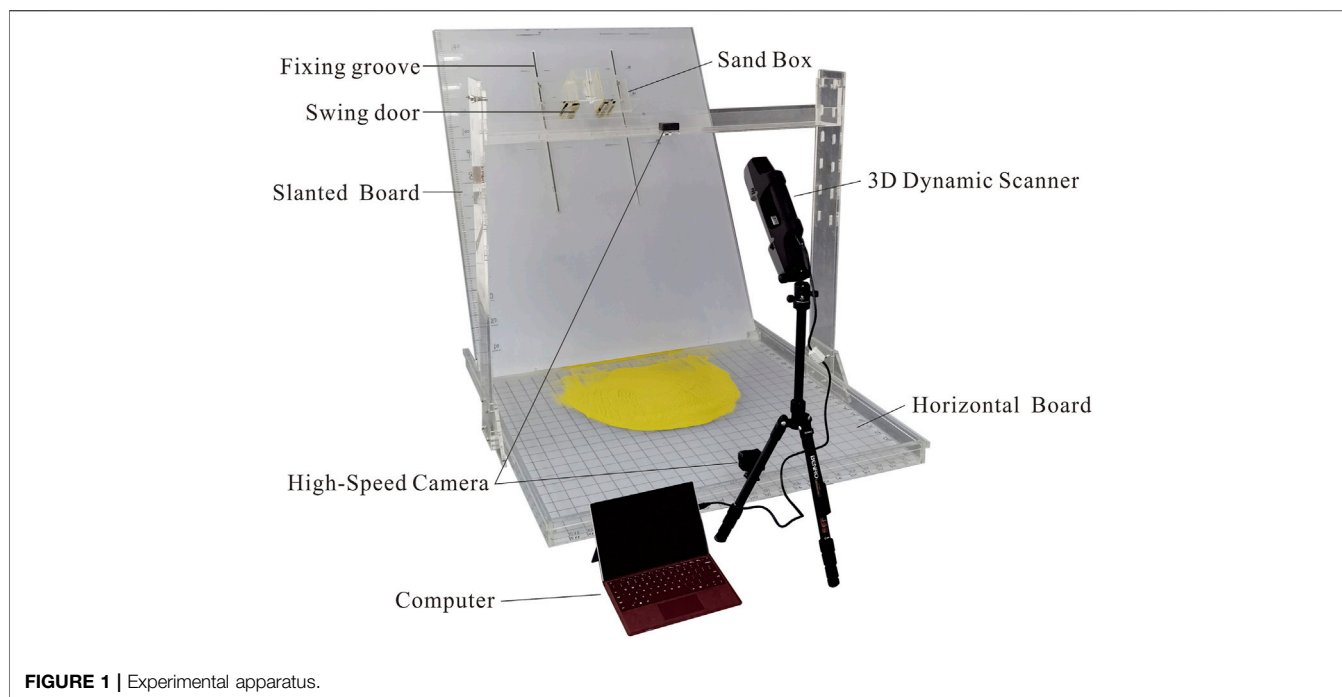


FIGURE 1 | Experimental apparatus.

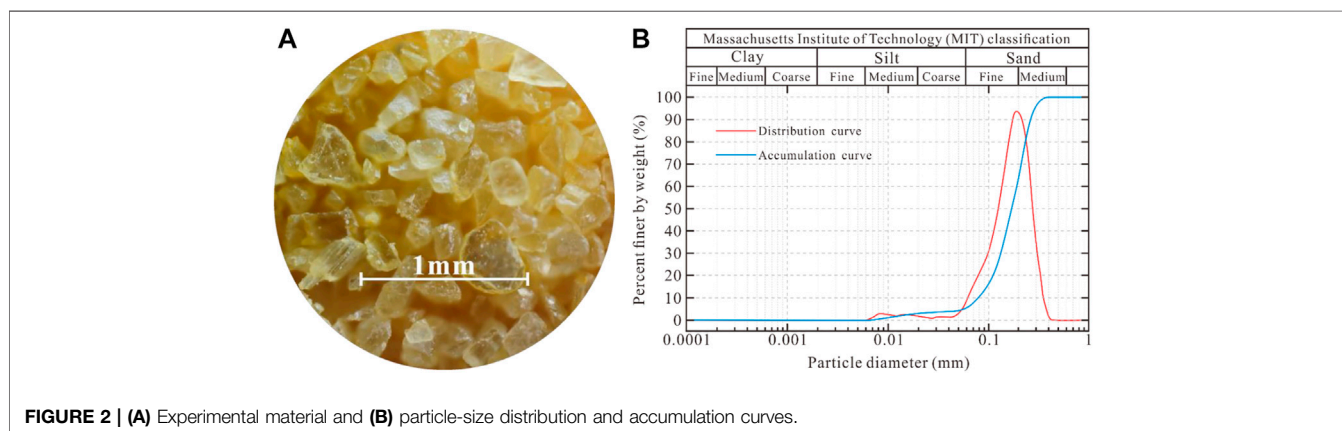


FIGURE 2 | (A) Experimental material and (B) particle-size distribution and accumulation curves.

2015), (Figure 2A). Its dry density was 1.5 g/cm^3 , its non-uniformity coefficient C_u was 2.39, and its curvature coefficient C_c was 1.19. The average diameter of sand particles was 0.2 mm and the specific surface area was $0.02 \text{ m}^2\text{kg}^{-4}$. The cumulative particle size percentage was 87.71% in the range of 0.075–0.5 mm. The internal friction angle ϕ was 33.86° and the cohesion C was 13.56. Particle size curves are shown in Figure 2B.

In this experiment, the friction coefficient between the sand and the slanted plate was tested by an improved direct shear test. This test is modified from the direct shear test by replacing the soil that would normally under the shear surface with Plexiglas. It is necessary to ensure frictional movement of the sand along the surface of the Plexiglas during shear. After graded pressurized shearing, the friction coefficient between the sand body and Plexiglas was measured to be 0.474.

Typical Movement Process

The whole landslide process was recorded by a high-speed camera and 3D scanner. Reverse modeling was carried out to restore the whole landslide process from the 3D scanner data. In the experiment, the landslide movement process was similar and the morphological changes in the sliding body were similar at different heights. Taking $H = 110 \text{ cm}$ as an example, the whole sliding process can be divided into two stages, as shown in Figure 3.

The first stage is the movement of the sliding body from the initial position to the point where the tip of the sliding body is in contact with the horizontal plate, a process that lasts about 500 ms. (Figure 3A–E). The slide exited the sandbox and moved along the slanted plate (A, B), during which time the slide unfolded first in the moving direction and thus formed an overall elongated shape with a wide front and narrow back (C–E). This may be the result of the unfolding occurring first in the

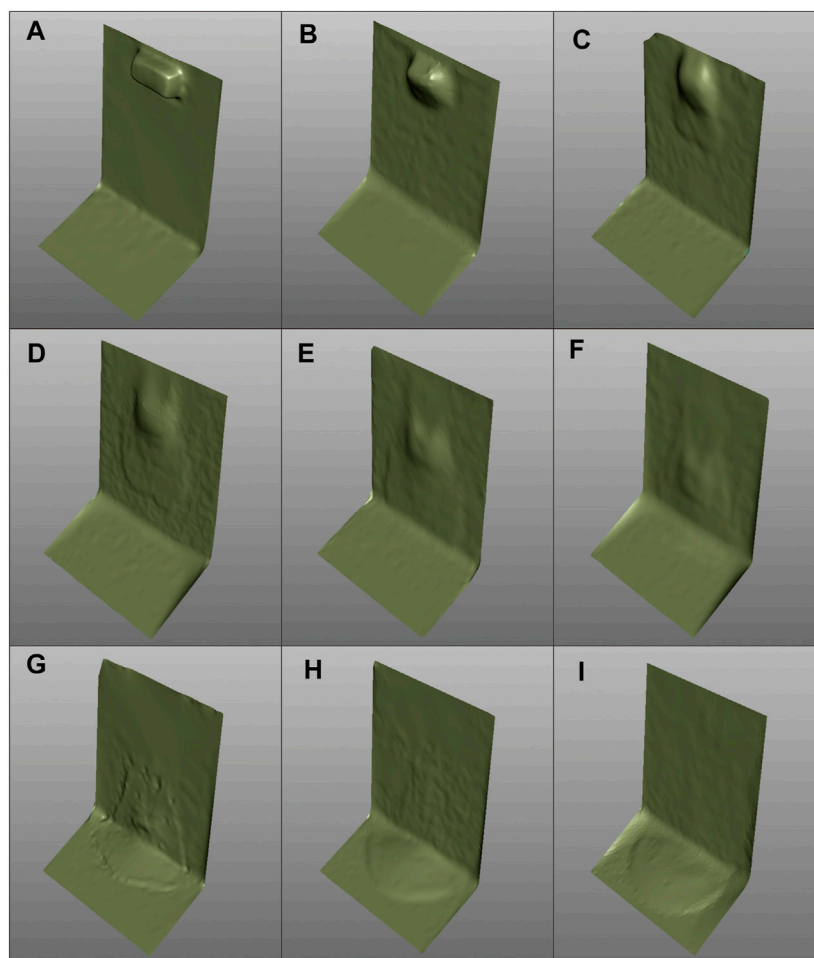


FIGURE 3 | Sliding process diagram.

sliding body directly adjacent to the slanted plate part and then gradually transferring to the area away from the slanted plate. The upper sliding body largely maintained its original form and remained in the rear position of the whole sliding body (this part eventually became the peak of the deposit).

The second stage was from the time when the tip of the slide contacted the horizontal plate to the time the end of the slide completely fell, and lasted about 500 ms (**Figure 3F–I**). When the tip of the sliding body contacted the horizontal plate, its spreading speed decreased significantly. Meanwhile, the sliding body at the slanted plate was still in the process of expansion; therefore, the overall length of the sliding body was in a state of slow elongation (F, G). At the same time, the part that maintained its original shape in the slanted plate stage also began to move towards the front of the sliding body and gradually expanded. When this part of the slide reached the plate, there was only a thin layer of residual slide (H) on the slanted plate. When this thin layer completely slid off, the whole slide stopped and the sliding process was complete (I).

The lower the landslide height H , the shorter the whole sliding process and the smaller the impact range of the whole landslide.

The differences in landslide length, width, height, and center of gravity from different drop heights will be discussed in detail later. For the convenience of discussion, a diagram of the landslide process's variables is shown in **Figure 4**.

RESULTS

Length of Sliding Body

Figure 5 shows the variation in sliding body length with drop height.

The curves of sliding body length with drop height are generally similar (**Figure 5A**). According to the two stages defined in *Typical movement process*, the length of the sliding body increases rapidly in the first stage, then grows slowly and shrinking rapidly in the second stage. The variations in sliding body length between different initial landslide heights are not significant in the first stage. In the second stage, differences in sliding body length began to appear; the length peaked after a slow increase, then narrowed as it rapidly shortened.

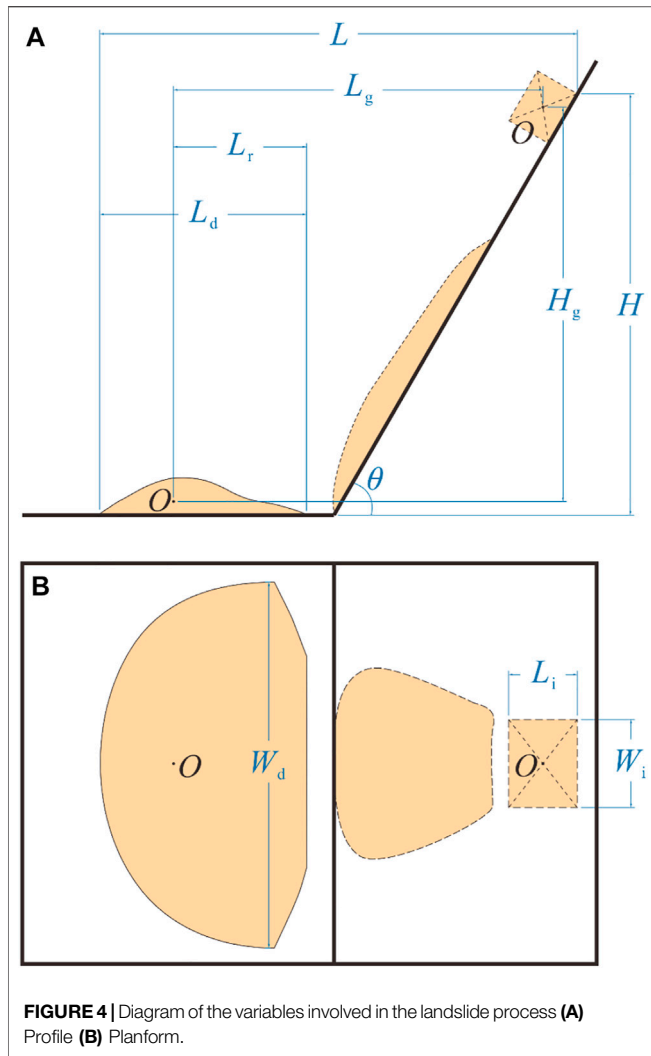


FIGURE 4 | Diagram of the variables involved in the landslide process **(A)** Profile **(B)** Planform.

By carefully observing the changes in the morphology of the sliding body throughout the landslide process, it was found that the reason for the change in sliding body length is that the tip of the slide advances rapidly in the first stage. Meanwhile, the trailing end of the slide advances slowly due to the unfolding of the bottom of the sliding body. When the landslide process enters the second stage, the tip of the sliding body impacts the bottom plate and slows down the landslide's advance due to energy loss, but it still advances slightly faster than the trailing end of the sliding body. The length of the sliding body, therefore, increases slowly. When most of the slide reaches the flat plate, the sliding body remaining on the sloping plate is thin. At this time, the back end of the sliding body falls rapidly, the length of the sliding body therefore rapid shortening.

Figure 5B shows that the higher the initial height, the longer the final sliding body length. The final length of the sliding body can be expressed as:

$$L_d = L_i + 0.338H \tag{1}$$

According to Eq. 1, the final length of the sliding body changes with the initial length, which is a linear increasing function starting from the initial length L . Since only a slope of $\theta = 60^\circ$ was considered in this study, the coefficient in Eq. 1 may vary with θ .

Width of Sliding Body

Figure 6A shows the variation in sliding body width with drop height.

The curves of the variations in sliding body width are generally similar. In the first stage of sliding, the sliding body width increases linearly and rapidly, and is relatively unaffected by the initial height. The sliding body width tends to maintain a constant value in the second stage and shows some variation with initial height.

The final sliding body widths at different initial heights are shown in Figure 6B and :

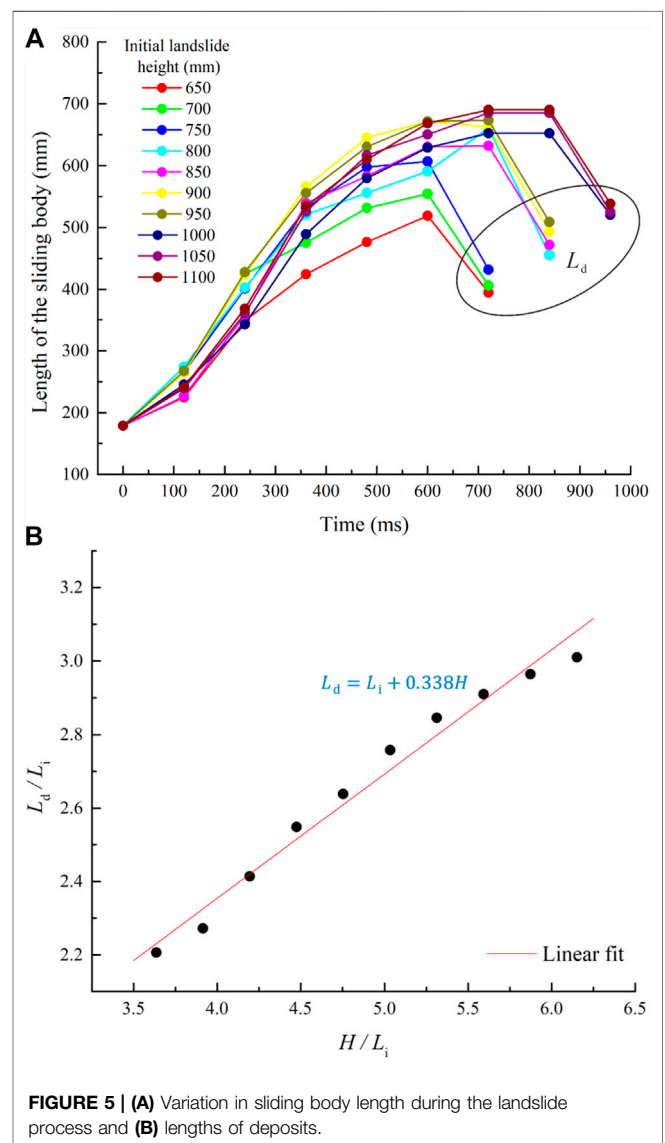


FIGURE 5 | **(A)** Variation in sliding body length during the landslide process and **(B)** lengths of deposits.

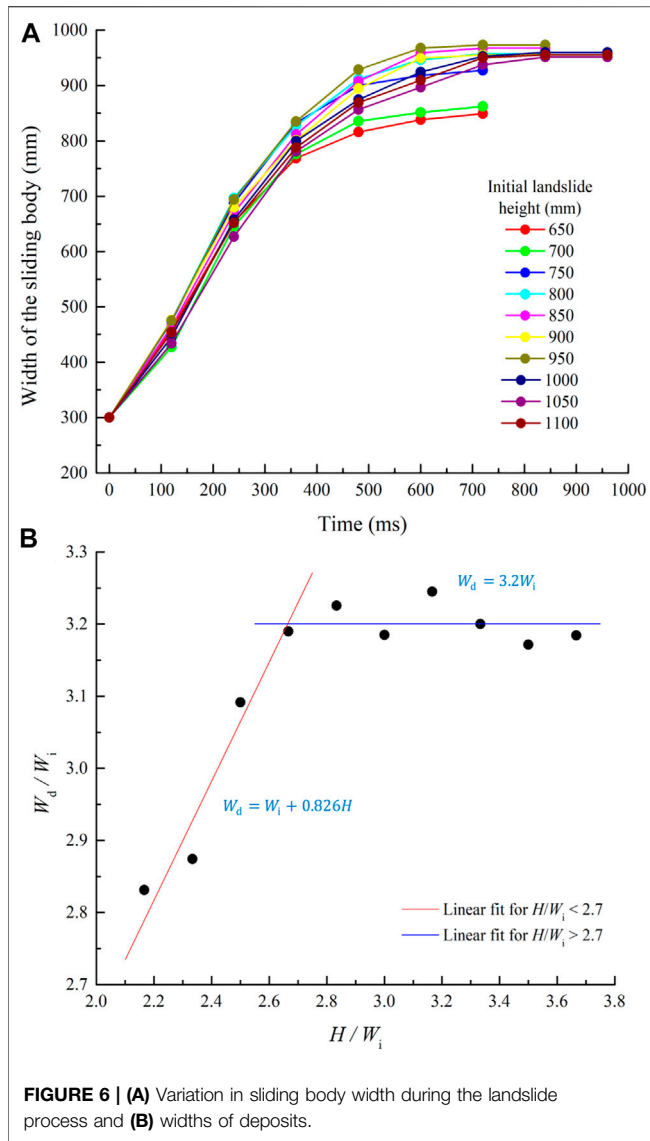


FIGURE 6 | (A) Variation in sliding body width during the landslide process and **(B)** widths of deposits.

$$\begin{cases} W_d = W_i + 0.826H & (H < 2.7W_i) \\ W_d = 3.2W_i & (H \geq 2.7W_i) \end{cases}, \quad (2)$$

Equation 2 is a piecewise function with significantly different values before and after the cut-off point $H = 2.7W_i$. When the drop height is low, the width of the sliding body follows a linearly increasing function starting from the initial width. When the height of the landslide is greater than 2.7 times the initial width, the final width of the sliding body is basically stable at 3.2 times the initial width. Since this study only considers a slope of 60° , the coefficient in the equation may change with θ .

Height of Sliding Body

The variations in sliding body height over time from different initial heights are shown in **Figure 7**.

Figure 7A compares the variations in sliding body height during the process of landslides from different initial heights. The curves have similar shapes. As with the change in length of the

sliding body, the height increases rapidly in the first stage, decreases slowly, and then decreases rapidly in the second stage. The sliding body height variation with initial height was not significant in the first stage. However, variation starts to appear in the second stage, reaches a maximum after some slow growth. The final height of the shortened sliding body is significantly less than the initial height of the sliding body.

As shown in **Figure 7B**, The equation for the final height of the sliding body is:

$$H_d = 0.526H_i - 0.063H, \quad (3)$$

Barycenter of Sliding Body

The barycenter of a landslide varies mainly in the sliding direction and little in the lateral direction. So, only changes in the center of

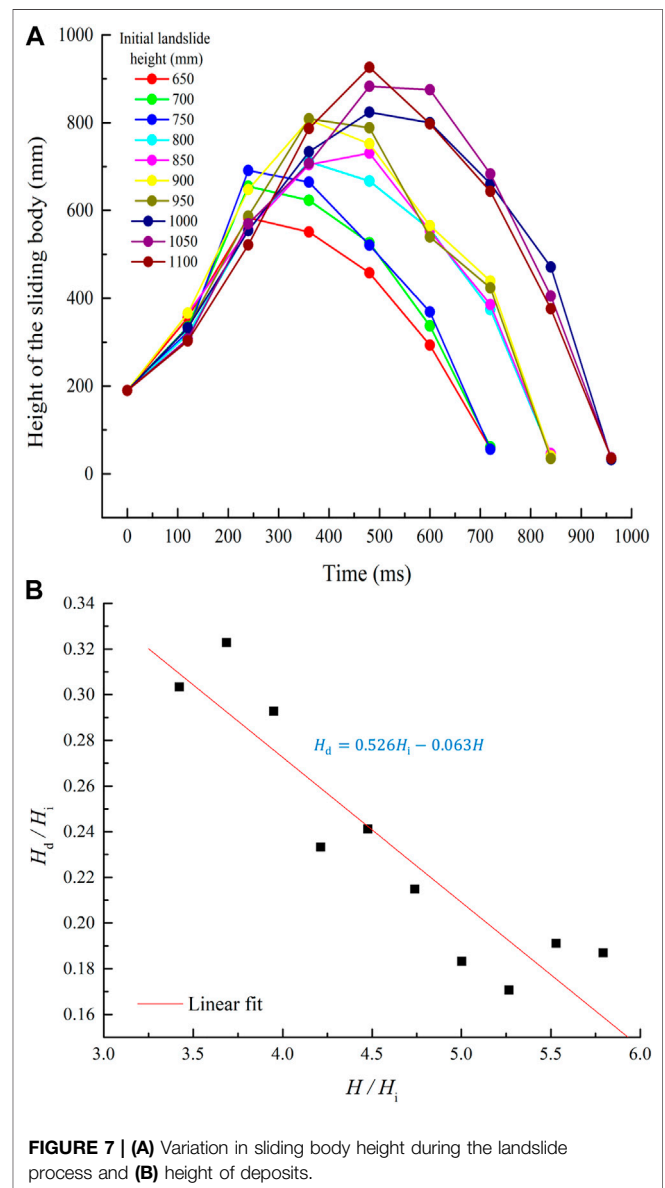
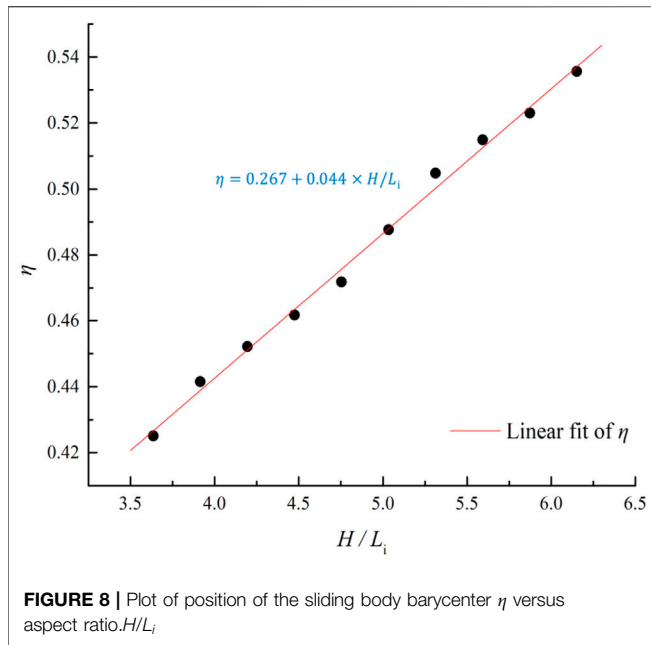


FIGURE 7 | (A) Variation in sliding body height during the landslide process and **(B)** height of deposits.



gravity in the sliding direction are discussed. The aspect ratio $\alpha = H/L_i$ is often used to describe the initial morphological characteristics of a slide and affects the final morphology of the slide (Crosta, Imposimato, and Roddeman; Phillips et al., 2006;2009; Lucas et al., 2011) This ratio can also be used as a factor to describe the position of the sliding body barycenter: $\eta = L_r/L_d$. The change in the sliding body barycenter position is shown in **Figure 8**.

As shown in **Figure 8**, η and H/L_i presents an obvious linear relationship that follows:

$$\eta = 0.267 + 0.044 \times H/L_i, \tag{4}$$

The growth in η in this experiment was linear. However, it is obvious that the value of η cannot exceed 1. Therefore, the growth trend of η will probably slow down or even decline instead of consistently increasing linearly. Since the maximum value of H/L_i in this experiment was about 6.15, further research is needed to determine the value of η under the circumstances $H/L_i > 6.15$.

DISCUSSION

Variation of Sliding Body

It can be seen from **Figures 5–7** that the sliding body undergoes a process of growth followed by decrease in the length and height directions, which is due to the change in the force state of the sliding body when it contacts the horizontal board. As a result of the change in the direction of support and frictional resistance, the sliding body is more impeded in the direction of falling and forward direction. The sliding body consequently starts to shorten in length and height from a stretched state and gradually stops the motion. The magnitude of the friction

coefficient in this process and its effects on the landslide height to length ratio will be discussed in the next section.

Unlike the variation in the length and height of the sliding body, the width gradually remains stable after an apparent increase. The sliding body is not subjected to external forces in the width direction during the whole process. The reason for its growth in the width direction is due to the shear stresses generated by the compression when gravity and support forces act on the sliding body. Meanwhile, because the sliding body is not subjected to external forces in the width direction throughout, the sliding body does not show significant shortening in this direction. Despite the fact that the changing regularity of the sliding body in width differs from that in length and height, the time point at which it tends to flatten out is consistent with the time point at which the length and height of the sliding body shorten.

Effective Friction Coefficient μ

In order to analyze the effective friction coefficient μ on the sliding surface, force analysis was carried out on the sliding body. The force analysis diagram is shown in **Figure 9**.

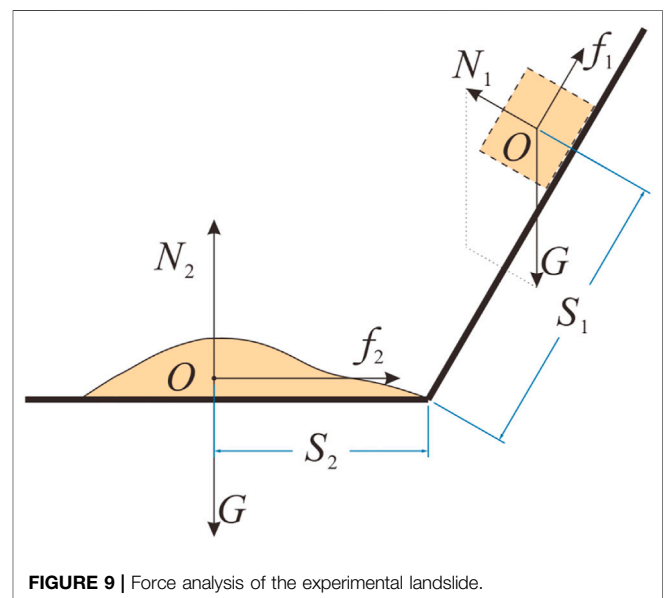
In the sliding stage, the sand body always moves along the direction of the slanted plate, so the resultant force it receives in the vertical direction of the slanted plate is zero, then:

$$G \times \cos\theta = N_1, \tag{5}$$

The combined force along the slanted plate is the component force of gravity in that direction and the friction between the slanted plate and the sliding body. So, in the direction of the slanted plate, there is:

$$F_1 = G \times \sin\theta - f_1, \tag{6}$$

The value of the frictional force is equal to the product of the friction coefficient μ and the support force N , i.e.:



$$f_1 = \mu \times N_1, \tag{7}$$

Since the size of the friction force is only related to the roughness of the contact surface and not to the contact area, and since the total gravity of the sliding body and the force between the sliding body and plate do not change during the landslide process, the total friction force between the sliding body and Plexiglas plate does not change during the landslide process.

By substituting Eqs 5, 7 into Eq. 6, we can obtain:

$$F_1 = G \times \sin\theta - \mu \times G \times \cos\theta = G \times (\sin\theta - \mu \times \cos\theta), \tag{8}$$

When the sliding body reaches the bottom and slides horizontally, the resultant force on the sand body in the vertical direction of the plate is zero and the force on the plate is the friction force f_2 between the plate and the sand body. Then:

$$G = N_2, \tag{9}$$

$$f_2 = \mu \times N_2, \tag{10}$$

$$F_2 = f_2, \tag{11}$$

Combining Eqs 9–11, we can obtain:

$$F_2 = \mu \times G, \tag{12}$$

When the sliding body reaches the plate, according to the law of conservation of energy:

$$F_1 \times S_1 = \frac{1}{2} m \times v_1^2, \tag{13}$$

At the moment when the sliding body hits the plate, it satisfies the momentum theorem in the vertical direction. The instantaneous impulse transfer process involves the energy loss as the sliding body hits the plate. The energy lost in the process is:

$$\Delta E_1 = \frac{1}{2} m \times (v_1 \times \sin\theta)^2, \tag{14}$$

Substituting Eq. 13 into Eq. 14, we can obtain:

$$\Delta E_1 = F_1 \times S_1 \times \sin^2\theta, \tag{15}$$

At the moment when the sliding body impacts the plate, in addition to the impact energy loss, there is also some energy loss due to an increase in horizontal friction due to increased impact pressure. Although the impact force is usually large, this part of the energy is very small compared with the energy loss of vertical impact because this time period is less than 0.02 s, and the sliding distance of the sliding body is also limited. Therefore, this component of energy loss is ignored.

According to the conservation of energy during the whole landslide process:

$$F_1 \times S_1 - \Delta E_1 = F_2 \times S_2, \tag{16}$$

Combining Eqs 8, 12, 15–17 can be obtained after simplification:

$$\mu = \frac{S_1 \times \sin\theta \times \cos^2\theta}{S_1 \times \cos^3\theta + S_2}, \tag{17}$$

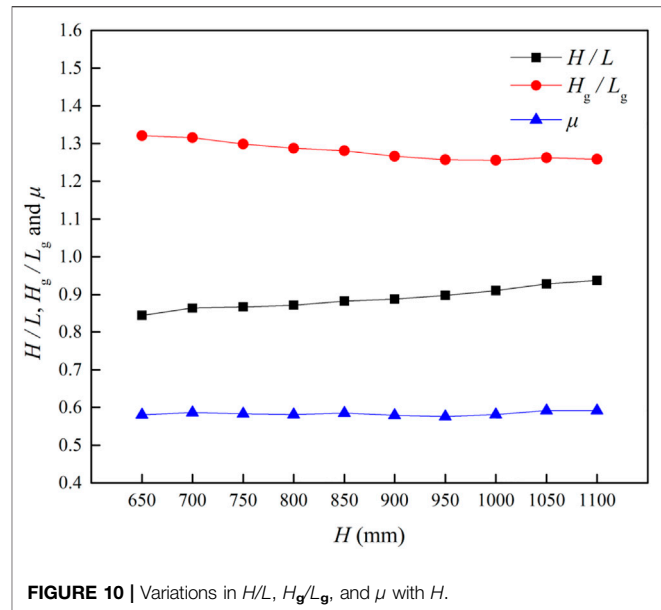


FIGURE 10 | Variations in H/L , H_g/L_g , and μ with H .

In this study, the volume of the sliding body, the initial shape of the sliding body, and the morphological characteristics of the sliding surface were all the same, therefore the errors caused by these factors were eliminated in the experiment. Therefore, the H/L , H_g/L_g and μ values were more stable than those obtained from real landslides. Figure 10 shows the H/L , H_g/L_g , and μ curves calculated from Eq. 18 for different values of H .

As can be seen from Figure 10, the value of H/L increases slowly with H . In contrast, H_g/L_g decreases slowly with increases in H . Only μ is relatively stable in relation to H . According to the direct shear test described in *Properties of sand samples*, the friction coefficient between the sliding body and slanted plate was 0.474, which is also closer to $\mu = 0.5834$ in Figure 10, while differing from the values of H/L and H_g/L_g .

Range of Landslide

The range of a landslide in the length direction is usually described in terms of the overall landslide length L , which we also use. Combined with the changes in the length of the sliding body discussed above and the position of the barycenter, it is reasonable to express the overall length of the landslide by

$$L = H/\tan\theta + S_2 + (1 - \eta) \times L_d, \tag{18}$$

In Eq. 18, the first term is the projection of the slope of the landslide, the second term is the movement distance of the barycenter in the horizontal stage, and the third term is the distance between the barycenter and the toe of the sliding body.

The displacement equation of the center of gravity at the plate stage can be derived from Eq. 17:

$$S_2 = \frac{S_1 \times \sin\theta \times \cos^2\theta}{\mu} - S_1 \times \cos^3\theta, \tag{19}$$

TABLE 1 | Summary of properties for the landslides from reality and experiments.

Data source	H	θ	S_1	μ	L_i	L Calculated by formula (18)	L In the original research
Duan LD01	56.10	40.73	44.60	0.48	33.80	115.53	117.40
Duan LD21	40.90	44.77	51.97	0.27	36.90	125.93	151.80
Duan LD13	83.50	45.00	107.06	0.33	75.70	232.89	256.10
Duan LD07	62.50	48.22	57.93	0.51	38.60	115.62	121.80
Duan LD39	54.30	48.36	42.29	0.45	28.10	96.99	120.60
Duan LD14	84.80	49.15	85.00	0.59	55.60	152.43	144.30
Duan LD16	90.10	58.03	79.33	0.69	42.00	118.26	131.50
Crosta's experimental results	77.13	40.00	105.00	0.70	33.27	138.75	128.56
	84.85	45.00	105.00	0.70	32.53	138.60	125.71
	91.93	50.00	105.00	0.70	31.54	134.59	131.32
	98.30	55.00	105.00	0.70	30.31	126.95	122.87
	103.92	60.00	105.00	0.70	28.86	116.11	109.39
	108.76	65.00	105.00	0.70	27.18	102.68	94.57

In Eq. 18, η and L_d can be calculated from Eqs 1, 4, respectively. When we know the displacement of the landslide barycenter, the position of the barycenter in the sliding body, and the possible expansion of the landslide body after the landslide, we can calculate the overall length of the landslide L and predict its possible range of impact. Before the occurrence of a landslide, the shape of the sliding body and position of the sliding surface can often be obtained *via* analysis, while the values of S_1 and θ in Eq. 19 can be obtained *via* modeling analysis. Variable μ is the friction coefficient at the sliding surface, and η and L_d are functions of H and L_i . These variables can be obtained before the occurrence of a landslide if the initial shape of the sliding body is known, so as to calculate S_2 , η , and L_d to predict the landslide length L according to Eq. 18.

The landslide's range of influence in the width direction is equivalent to the final width of the landslide body, as described by Eq. 2. It is meaningful to study the change in width of the landslide body, because width and length changes are both important parts of the impact range. In some areas threatened by geological hazards such as landslides and collapses, residents need to be relocated. The width of the landslide is an important factor determining the number of residents to be relocated.

The range of the landslide in the height direction is shown by Eq. 3. Because the scope of a landslide hazard is usually only determined by the length and width while the height has little influence, there are few studies on this aspect.

Although the volume of the sliding body V is not reflected in Eqs 2, 3, 18, the influence of sliding body volume on the movement ability of a landslide is contained in the form of L_i , W_i , and T_i . It is obvious that even if the volumes of landslides are the same, different shapes can lead to different movement capacities and ranges. Therefore, an equation containing L_i , W_i , and T_i parameters may be a better way to express the landslide movement ability than one only based on the volume of the sliding body V . Further research on the movement ability of landslides with different initial shapes will be the next research focus, which will help to

further improve the sliding distance equation determined in this study.

Comparison With Previous Studies

Many studies have included a variety of experimental as well as real landslide statistics. However, because the formulae in this research require many parameters that have received less attention, the statistics in many of the relevant papers are difficult to compare with the results in this paper. For example, Johnson (Johnson and Campbell 2017) focused on the relationship between slide volume and H/L in his paper, while the initial shape of the sliding body and the slide angle were not described in detail. Lucas (Lucas et al., 2011; Lucas, Mangeney, and Ampuero 2014) provided a summary of geomorphic data for large Martian landslides, but the values of the landslide slope in his research are mostly situated between 5 and 30°, which deviates significantly from the 60° in this paper. After screening the data from multiple papers, the actual landslide data from Duan's research (Duan, Cheng, et al., 2021) and the experimental data from Crosta's research (Crosta et al., 2017) are finally selected to compare with the results from this paper, as shown in Table 1.

It should be noted that only data for landslides with slope angles between 40 and 80° are presented, because excessive angle differences can make the comparison meaningless. To make the data applicable to Eq. 18, the value of μ are approximately use the value of H/L , and the values of and S_1 in Duan's article (Duan, Cheng, et al., 2021) was calculated by the following approximate equations:

$$\theta = \arctan(H_i/L_i), \quad (20)$$

$$S_1 = L_i/\cos\theta, \quad (21)$$

Since Crosta et al.'s data H , θ , S_1 and L_i were obtained from the experimental apparatus and experimental design. Because a slope of less than 30° was insufficient for flowage in their experiment and only the experimental data with slope angle greater than 40° were presented, the friction angle is therefore assumed to be 35° and the friction coefficient is accordingly 0.7. By comparison, we can find that the results of Eq. 18 are closer to those of Crosta and Duan. However, the comparative data provided in this paper contain some estimates in the calculations as well as are still quantitatively insufficient. The authors will refine the equation

further by performing more precise statistics and calculations based on future landslide data.

CONCLUSION

Through a series of experiments, this paper studied the movement of landslides of different heights, deformation of the sliding body and the movement distance of the barycenter. We proposed an equation describing the landslide range, which are helpful to understand the movement of some landslides. Based on the experimental observations, results, and analysis, the main conclusions are as follows:

- 1) In the experiment, the movement processes of landslides with different initial heights were found to be similar, as were the morphological changes in the landslide body. The whole landslide process took about 1,000 ms. The lower the landslide height, the shorter the duration of the whole sliding process and the smaller the landslide impact area. During the process of landslide, the length of the sliding body increases linearly from its initial length; the width of the sliding body is gradually maintained after growth; the height of the sliding body decreases with increases in landslide height.
- 2) The barycenter of the sliding body pushes toward the front of the slide as the height of the slide increases; however, determination of the barycenter's location in the final sliding body needs further study for cases of $H/L_1 > 6.15$. Displacement of the barycenter can be determined by the

energy conservation theorem, if the friction coefficient μ could be obtained experimentally.

- 3) The length of a landslide can be estimated by Eq. 18 in this paper. The landslide length prediction equation proposed in this paper is closer to the actual landslide distance at about 60° , but the validation data that the authors found are still insufficient, and more cases are necessary to support the formula in the future.

DATA AVAILABILITY STATEMENT

The raw data supporting the conclusions of this article will be made available by the authors, without undue reservation.

AUTHOR CONTRIBUTIONS

Experiments: HL, YW, and CD. Drafting the paper: HL. Make important revisions to the paper: ZD and FZ. For approval to the final version of the paper: ZD.

FUNDING

This study would not have been possible without financial support from the Special Fund for the National Natural Science Foundation of China under Grant nos. 41790442, 41702298 and 41602359, as well as the Project Supported by Natural Science Basic Research Plan in Shaanxi Province of China under Grant no. 2017JQ4020.

REFERENCES

- Aaron, J., Hungr, O., Stark, T. D., and Baghdady, A. K. (2017). Oso, Washington, Landslide of March 22, 2014: Dynamic Analysis. *J. Geotech. Geoenviron. Eng.* 143 (9), 05017005. doi:10.1061/(ASCE)GT.1943-5606.0001748
- Berger, C., McArdell, B. W., and Schlunegger, F. (2011). Direct Measurement of Channel Erosion by Debris Flows, Illgraben, Switzerland. *J. Geophys. Res.* 116 (F01002), a–n. doi:10.1029/2010JF001722
- Bouchut, F., Fernández-Nieto, E. D., Mangeney, A., and Narbona-Reina, G. (2015). A Two-phase Shallow Debris Flow Model with Energy Balance. *Esaim: M2an* 49 (1), 101–140. doi:10.1051/m2an/2014026
- Corominas, J. (1996). The Angle of Reach as a Mobility Index for Small and Large Landslides. *Can. Geotech. J.* 33 (2), 260–271. doi:10.1139/t96-005
- Crosta, G. B., De Blasio, F. V., De Caro, M., Volpi, G., Imposimato, S., and Roddeman, D. (2017). Modes of Propagation and Deposition of Granular Flows onto an Erodible Substrate: Experimental, Analytical, and Numerical Study. *Landslides* 14 (1), 47–68. doi:10.1007/s10346-016-0697-3
- Crosta, G. B., De Blasio, F. V., Locatelli, M., Imposimato, S., and Roddeman, D. (2015). Landslides Falling onto a Shallow Erodible Substrate or Water Layer: An Experimental and Numerical Approach. *JOP Conf. Ser. Earth Environ. Sci.* 26 (1), 012004. doi:10.1088/1755-1315/26/1/012004
- Crosta, G. B., Imposimato, S., and Roddeman, D. (2009). Numerical Modeling of 2-D Granular Step Collapse on Erodible and Non-erodible Surface. *J. Geophys. Res.* 114 (F3), F03020. doi:10.1029/2008JF001186
- Duan, Z., Cheng, W.-C., Peng, J.-B., Rahman, M. M., and Tang, H. (2021). Interactions of Landslide Deposit with Terrace Sediments: Perspectives from Velocity of Deposit Movement and Apparent Friction Angle. *Eng. Geology* 280, 105913. doi:10.1016/j.enggeo.2020.105913
- Duan, Z., Wu, Y.-B., Tang, H., Ma, J.-Q., and Zhu, X.-H. (2020). An Analysis of Factors Affecting Flowslide Deposit Morphology Using Taguchi Method. *Adv. Civil Eng.* 2020, 1–14. doi:10.1155/2020/8844722
- Duan, Z., Yan, X., Sun, Q., Tan, X., and Dong, C. (2021). Effects of Water Content and Salt Content on Electrical Resistivity of Loess. *Environ. Earth Sci.* 80 (14), 469. doi:10.1007/s12665-021-09769-2
- Dufresne, A. (2012). Granular Flow Experiments on the Interaction with Stationary Runout Path Materials and Comparison to Rock Avalanche Events. *Earth Surf. Process. Landforms* 37 (14), 1527–1541. doi:10.1002/esp.3296
- Evans, S. G., and Clague, J. J. (1994). Recent Climatic Change and Catastrophic Geomorphic Processes in Mountain Environments. *Geomorphology* 10 (1–4), 107–128. doi:10.1016/b978-0-444-82012-9.50012-8
- Geertsema, M., Clague, J. J., Schwab, J. W., and Evans, S. G. (2006). An Overview of Recent Large Catastrophic Landslides in Northern British Columbia, Canada. *Eng. Geology* 83 (1–3), 120–143. doi:10.1016/j.enggeo.2005.06.028
- Hungr, O. (2006). *Rock Avalanche Occurrence, Process and Modelling*. Dordrecht, Netherlands: Landslides from Massive Rock Slope Failure, 243–266. doi:10.1007/978-1-4020-4037-5_14
- Iverson, R. M., George, D. L., and Logan, M. (2016). Debris Flow Runup on Vertical Barriers and Adverse Slopes. *J. Geophys. Res. Earth Surf.* 121 (12), 2333–2357. doi:10.1002/2016JF003933
- Johnson, B. C., and Campbell, C. S. (2017). Drop Height and Volume Control the Mobility of Long-Runout Landslides on the Earth and Mars. *Geophys. Res. Lett.* 44 (24), 12,091–12,097. doi:10.1002/2017GL076113
- Kim, G.-B., Cheng, W., Sunny, R. C., Horrillo, J. J., McFall, B. C., Mohammed, F., et al. (2020). Three Dimensional Landslide Generated Tsunamis: Numerical and Physical Model Comparisons. *Landslides* 17 (5), 1145–1161. doi:10.1007/s10346-019-01308-2
- Legros, François. (2002). The Mobility of Long-Runout Landslides. *Eng. Geology* 63 (3–4), 301–331. doi:10.1016/S0013-7952(01)00090-4

- Lucas, A., Mangeney, A., and Ampuero, J. P. (2014). Frictional Velocity-Weakening in Landslides on Earth and on Other Planetary Bodies. *Nat. Commun.* 5 (1), 3417. doi:10.1038/ncomms4417
- Lucas, A., Mangeney, A., Mège, D., and Bouchut, F. (2011). Influence of the Scar Geometry on Landslide Dynamics and Deposits: Application to Martian Landslides. *J. Geophys. Res.* 116 (E10), E10001. doi:10.1029/2011JE003803
- Magnarini, G., Mitchell, T. M., Grindrod, P. M., Goren, L., and Schmitt, H. H. (2019). Longitudinal Ridges Imparted by High-Speed Granular Flow Mechanisms in Martian Landslides. *Nat. Commun.* 10 (1), 4711. doi:10.1038/s41467-019-12734-0
- Ng, C. W. W., Choi, C. E., Goodwin, G. R., and Cheung, W. W. (2017). Interaction between Dry Granular Flow and Deflectors. *Landslides* 14 (4), 1375–1387. doi:10.1007/s10346-016-0794-3
- Okura, Y., Kitahara, H., and Sammori, T. (2000). Fluidization in Dry Landslides. *Eng. Geology* 56 (3–4), 347–360. doi:10.1016/S0013-7952(99)00118-0
- Okura, Y., Kitahara, H., Sammori, T., and Kawanami, A. (2000). The Effects of Rockfall Volume on Runout Distance. *Eng. Geology* 58 (2), 109–124. doi:10.1016/S0013-7952(00)00049-1
- Opiso, E. M., Puno, G. R., Albuero, J. L. P., and au, A. L. (2016). Landslide Susceptibility Mapping Using GIS and FR Method along the Cagayan de Oro-Bukidnon-Davao City Route Corridor, Philippines. *KSCE J. Civ Eng.* 20 (6), 2506–2512. doi:10.1007/s12205-015-0182-x
- Phillips, J., Hogg, A., Kerswell, R., and Thomas, N. (2006). Enhanced Mobility of Granular Mixtures of Fine and Coarse Particles. *Earth Planet. Sci. Lett.* 246 (3), 466–480. doi:10.1016/j.epsl.2006.04.007
- Pudasaini, S. P., and Jaboyedoff, M. (2020). A General Analytical Model for Superelevation in Landslide. *Landslides* 17 (6), 1377–1392. doi:10.1007/s10346-019-01333-1
- Scheidegger, A. E. (1973). On the Prediction of the Reach and Velocity of Catastrophic Landslides. *Rock Mech.* 5 (4), 231–236. doi:10.1007/BF01301796
- Staron, L. (2008). Mobility of Long-Runout Rock Flows: A Discrete Numerical Investigation. *Geophys. J. Int.* 172 (1), 455–463. doi:10.1111/j.1365-246X.2007.03631.x
- Viroulet, S., Sauret, A., Kimmoun, O., and Kharif, C. (2013). Granular Collapse into Water: Toward Tsunami Landslides. *J. Vis.* 16 (3), 189–191. doi:10.1007/s12650-013-0171-4
- Wang, Gonghui., Sassa, Kyoji., and Fukuoka, Hiroshi. (2003). “Downslope Volume Enlargement of a Debris Slide–Debris Flow in the 1999 Hiroshima, Japan, Rainstorm. *Eng. Geology* 69 (3–4), 309–330. doi:10.1016/S0013-7952(02)00289-2
- Wang, Y.-F., Xu, Q., Cheng, Q.-G., Li, Y., and Luo, Z.-X. (2016). Spreading and Deposit Characteristics of a Rapid Dry Granular Avalanche across 3D Topography: Experimental Study. *Rock Mech. Rock Eng.* 49 (11), 4349–4370. doi:10.1007/s00603-016-1052-7
- Xu, Q., Li, H., He, Y., Liu, F., and Peng, D. (2019). Comparison of Data-Driven Models of Loess Landslide Runout Distance Estimation. *Bull. Eng. Geol. Environ.* 78 (2), 1281–1294. doi:10.1007/s10064-017-1176-3
- Yan, X., Duan, Z., and Sun, Q. (2021). Influences of Water and Salt Contents on the Thermal Conductivity of Loess. *Environ. Earth Sci.* 80 (2), 52. doi:10.1007/s12665-020-09335-2
- Yang, H. Q., Xing, S. G., Wang, Q., and Li, Z. (2018). Model Test on the Entrainment Phenomenon and Energy Conversion Mechanism of Flow-like Landslides. *Eng. Geology* 239, 119–125. doi:10.1016/j.enggeo.2018.03.023
- Yang, Q., Cai, F., Ugai, K., Yamada, M., Su, Z., Ahmed, A., et al. (2011). Some Factors Affecting Mass-Front Velocity of Rapid Dry Granular Flows in a Large Flume. *Eng. Geology* 122 (3–4), 249–260. doi:10.1016/j.enggeo.2011.06.006
- Zhou, J.-w., Cui, P., and Yang, X.-g. (2013). Dynamic Process Analysis for the Initiation and Movement of the Donghekou Landslide-Debris Flow Triggered by the Wenchuan Earthquake. *J. Asian Earth Sci.* 76, 70–84. doi:10.1016/j.jseas.2013.08.007
- Zou, Z., Xiong, C., Tang, H., Criss, R. E., Su, A., and Liu, X. (2017). Prediction of Landslide Runout Based on Influencing Factor Analysis. *Environ. Earth Sci.* 76 (21), 723. doi:10.1007/s12665-017-7075-x

Conflict of Interest: The authors declare that the research was conducted in the absence of any commercial or financial relationships that could be construed as a potential conflict of interest.

Publisher’s Note: All claims expressed in this article are solely those of the authors and do not necessarily represent those of their affiliated organizations, or those of the publisher, the editors and the reviewers. Any product that may be evaluated in this article, or claim that may be made by its manufacturer, is not guaranteed or endorsed by the publisher.

Copyright © 2021 Li, Duan, Wu, Dong and Zhao. This is an open-access article distributed under the terms of the Creative Commons Attribution License (CC BY). The use, distribution or reproduction in other forums is permitted, provided the original author(s) and the copyright owner(s) are credited and that the original publication in this journal is cited, in accordance with accepted academic practice. No use, distribution or reproduction is permitted which does not comply with these terms.